atmosphere

MDPI

Article

Sensitivity Analysis of Modelled Air Pollutant Distribution around Buildings under Different Meteorological Conditions

Anton Petrov *, Emilia Georgieva and Elena Hristova

National Institute of Meteorology and Hydrology, 1784 Sofia, Bulgaria; emilia.georgieva@meteo.bg (E.G.); elena.hristova@meteo.bg (E.H.)

* Correspondence: anton.petrov@meteo.bg

Abstract: The distribution of air pollutants in urban areas is significantly influenced by the presence of various geometric structures, including buildings, bridges, and tunnels. In built-up environments, meteorological conditions may influence the accumulation or dispersion of air pollutants in specific zones. This study examines the impact of wind and atmospheric stability on the dispersion of air pollutants around an apartment building situated in close proximity to a busy boulevard in a residential district of Sofia, Bulgaria. A series of dispersion simulations were conducted using the Graz Lagrangian Model (GRAL v.22.09) for a range of meteorological conditions, defined as combinations of the direction and velocity of the approaching flow, and of stability conditions within the study area of 1 × 1 km, with a horizontal resolution of 2 m. The resulting spatial distribution revealed the presence of hotspots and strong gradients in the concentration field. A simulation with meteorological data was also conducted, which was aligned with a campaign to monitor vehicular traffic. The sensitivity tests indicate that GRAL is capable of reproducing high-resolution pollutant fields, accounting for building effects at relatively low computational costs. This makes the model potentially attractive for city-wide simulations as well as for air pollution exposure estimation.

Keywords: wind; atmospheric stability; urban area; transport; Lagrangian dispersion model

Citation: Petrov, A.; Georgieva, E.; Hristova, E. Sensitivity Analysis of Modelled Air Pollutant Distribution around Buildings under Different Meteorological Conditions. *Atmosphere* **2024**, *15*, 638. https://doi.org/10.3390/atmos15060638

Academic Editors: Zhaobin Sun, Jun Yang and Ling Han

Received: 30 April 2024
Revised: 23 May 2024
Accepted: 23 May 2024
Published: 25 May 2024

1. Introduction

The rapid development of computing power over the last two decades has made it possible to solve problems at speeds that were previously unimaginable [1,2]. This is particularly true for computations related to various phenomena in the atmosphere, especially at local scale and microscale [3,4]. In built-up environments, where the fields of the different meteorological elements are characterised by strong spatial gradients, the distribution of pollutants becomes challenging for modellers and less predictable in character [5–8]. Blocks of flats in close proximity to busy roads act as a natural barrier against the infiltration of exhaust gases from vehicles into the spaces between the blocks. This inevitably leads to large differences in pollutant concentrations around the buildings [5,8,9]. The meteorological conditions on the microscale can influence the distribution of vehicle-emitted pollutants in both favourable and extremely unfavourable directions, relevant to the concentration of pollutants in the vicinity of people's everyday lives.

A plethora of studies have been conducted globally on the modelling of pollutant concentrations in urban areas, with particular consideration to the effects of various elements (street canyons, tunnels, intersections, etc.) e.g., [10–14]. The approaches employed exhibit a range of degrees of complexity, including semi-empirical models [15,16], dispersion models with specific parameterisations for the urban area [17], Lagrangian models [18,19], chemical transport models (CTMs) coupled with microscale Lagrangian or Gaussian models [20,21], and complex computational fluid dynamics (CFDs) models [3,14,22–25]. Semi-empirical models, exemplified by the Operational Street Pollution Model (OSPM) [16], make prior assumptions about flow and dispersion conditions within street canyons based on experimental data. They require minimal computational resources but have difficulty reproducing

variations in concentration in a changing built environment [26]. Gaussian models, such as the Atmospheric Dispersion Modelling System (ADMS) [17], may be employed to model an entire city or a portion thereof. They are frequently used in regulatory applications. However, they exhibit limited capabilities in representing the effects of obstacles to the flow and dispersion in urban areas and are unable to provide high-resolution spatial distributions of pollutants [27]. The integration of the CTM with a Lagrangian model, such as the microscale hybrid modelling system HMS [20], appears to be a suitable approach for conducting long-term city-wide, building-resolved air quality simulations. CFD models permit the generation of high-resolution simulations of complex flow and dispersion (for approximately a few metres), while accounting for various elements of the urban environment. However, they are characterised by high computational requirements. Their application is limited to long-term simulations, and certain restrictions must be considered, such as the passive scalar treatment of pollutants and neutral stratification [14].

A common problem for microscale CFD urban models is the proper specification of the initial and boundary conditions, as the traditional input from single-point observations does not represent the variability of the meteorological elements even in a small part of the city [28]. To deal with this issue, a combination of a mesoscale meteorological model with a fine-scale obstacle-resolving CFD model was found to provide realistic flow fields with resolution of a few metres [28–30]. A combined model system for obstacle-resolving dispersion simulations in urban areas might consist of single models with varying complexity. For example, the modelling system Graz mesoscale model (GRAMM)/Graz Lagrangian model (GRAL) [18,31,32] combines a mesoscale nonhydrostatic model, microscale flow model and a Lagrangian particle model. Designed to be efficient for long-term dispersion calculations [33], the system makes use of a catalogue approach, with pre-defined meteorological conditions for the large-scale forcing expressed in terms of wind and atmospheric stability.

In Europe, applications of models at the microscale (horizontal resolution of a few metres in urban areas) were also driven under the policy context of the Ambient Air Quality Directive [34], in order to identify hotspots with poor air quality and to provide support for measures in urban planning and plans for air quality improvement. The application of models of different complexity for estimating NO_2 long-term concentrations with high spatial resolution is discussed in a recent model inter-comparison study for a European city [27]. The authors underline that the spatial distribution for the monthly concentration is well reproduced by all methodologies (simple and complex models), but the main differences are in the gradients looking at different time and spatial scales.

In Bulgaria, air pollution modelling in urban environments is typically conducted within the context of applied research by scientific institutions or by consulting companies engaged in the elaboration of programmes for air quality improvement at the municipality level. Consequently, the models employed exhibit varying degrees of complexity. For example, a CTM approach is used for the city of Sofia, where results from the Bulgarian Chemical Weather Forecast System (BCWFS) over the national territory with a grid spacing of 9 km are downscaled through nested modelling domains to the city level with a resolution of 1 km [35,36]. Less complex numerical models (such as Gaussian or Lagrangian type) are applied in the operational system for air quality management in the second largest city in the country (Plovdiv) [37], in studies for assessment of the air pollution in Sofia [38], and in the preparation of air quality plans for Sofia Municipality [39]. A key limiting factor in the modelling results at a city scale is the lack of detailed information for the distribution of the emissions from sources that are highly variable in space—from traffic and from biomass burning for residential heating. These applications do not consider microscale processes where the flow and dispersion of pollutants are affected by urban structures (buildings, streets, etc.). The use of complex microscale models (CFD type) that allow spatial resolution down to a few metres and account for the effects of the built environment on the flow and dispersion of pollutants is still relatively uncommon in Bulgaria. First attempts in this direction were carried out recently by the [40,41] for cases of idealised street canyons and of a specific experimental campaign conducted in Germany [42]. These simulations

allowed us to check the computational requirements and their suitability for more detailed air pollution modelling for Sofia. As a further step and as a pilot study for Bulgaria, here we focused on test cases for high-resolution obstacle-resolving dispersion simulations in a small part of Sofia.

The aim of this work is to investigate the effect of wind direction and atmospheric stability on the distribution of pollutants around a block of flats located near a traffic road in a residential district of Sofia, Bulgaria. The modelling approach is based on the application of the GRAMM/GRAL model system for a built-up zone of 1 × 1 km and resolutions of 30 m and 2 m, respectively. The focus is on the spatial distribution of pollutant concentrations (nitrogen oxides (NO_X)) for different meteorological conditions, expressed as pre-defined combinations of wind and atmospheric stability. Results from the numerical experiments (test cases) have been analysed, considering changes in the spatial pattern, the gradients, and the magnitudes of the concentrations. In addition, a simulation was conducted using real meteorological data from the National Institute of Meteorology and Hydrology (NIMH) for a period of a few days. The resulting model outputs were then compared to data from a nearby regulatory air quality station.

2. Data and Methods

In this section, we outline first some air quality issues for Sofia, which were motivating regarding the selection of a modelling system and the numerical experiments on the dispersion of pollutants in a small part of the city. Then, a brief description of the model system, GRAMM/GRAL, is provided. Finally, details of the model input data and numerical experiments are presented. Figure 1 describes the methodology followed in this study.

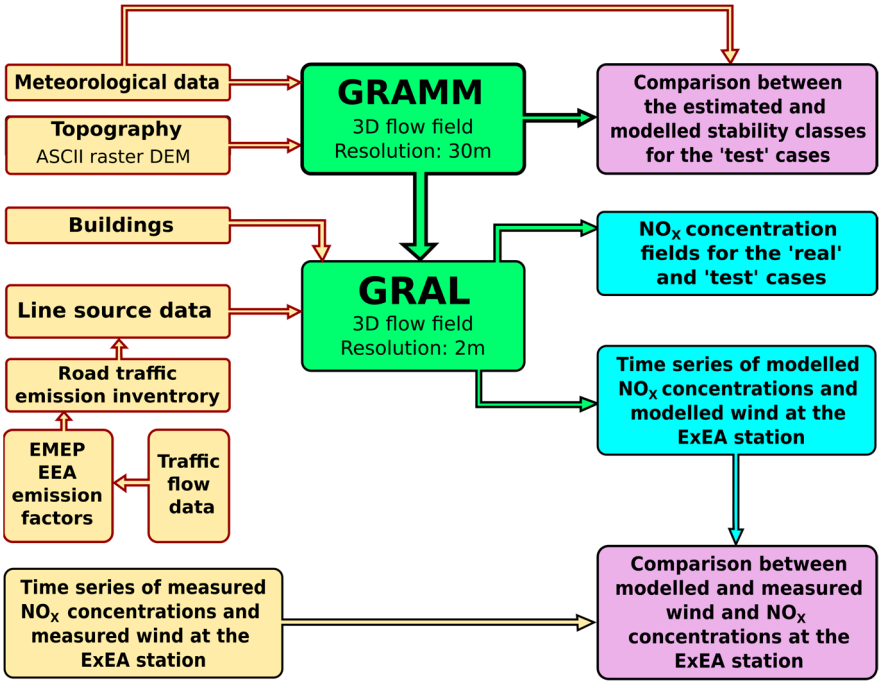

Figure 1. Flowchart of the methodology employed in the numerical experiments.

2.1. Sofia: Primary Air Quality Issues

Sofia, located in western Bulgaria, is the capital of the country with more than 1.2 million inhabitants. The city (with a total area of 1344 km^2) is situated in a valley oriented in an almost northwest-to-southeast direction (Figure 2a). The regulatory air quality network consists of five monitoring stations, one of them in the vicinity of a small part of the city, which was selected for the numerical simulations in this work (Figure 2b).

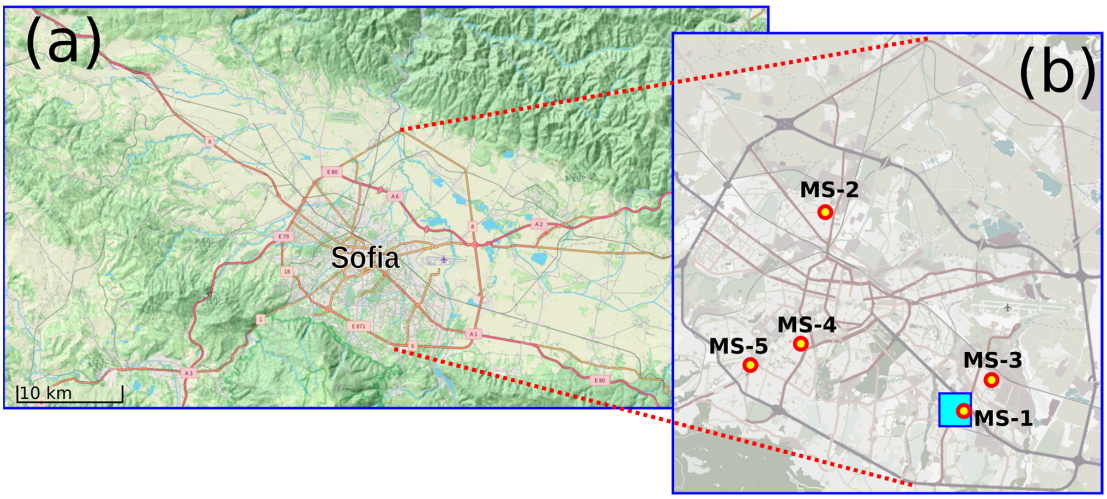

Figure 2. (**a**) Sofia Valley and surrounding mountains (adapted from OpenStreetMap). (**b**) A magnified image of Sofia City, indicating the locations of the pollution monitoring sites operated by the Executive Environmental Agency (ExEA). The blue square indicates the extent of the modelling domain.

The geographical position of Sofia and the orientation of the valley determine the wind regime, with prevailing flow from western and eastern directions and a significant percentage (48.8%) of calm winds (Figure 3). Especially in the winter season, the windless conditions increase the tendency for the accumulation of various types of air pollutants, emitted predominantly by anthropogenic activities [39].

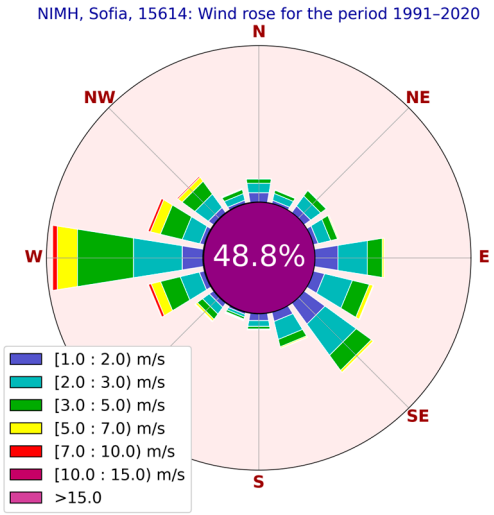

Figure 3. Wind rose for Sofia—Central Meteorological Station at NIMH for the climate period (1991–2020).

Air quality (AQ) problems in the city have been analysed based on monitoring and modelling data for purposes of municipality plans and measures for AQ improvement [39] and recently related to the introduction of Low-Emission Zones (LEZs) in Sofia's central part [43,44]. The conclusions point out problems with the concentrations of particulate matter (with diameters up to 2.5 μm ($PM_{2.5}$) and 10 μm (PM_{10})) and nitrogen dioxide (NO_2).

The mean annual NO_2 concentrations at the five regulatory AQ stations are in the range of 19.9–30.6 μg m^{-3} (2022) and 16.5–28.4 μg m^{-3} (2023). These values are below the annual limit value (40 μg m^{-3}) established by the European Ambient Air Quality Directive (AAQD) [34]. However, they are up to three times higher than the guidance value (10 μg m^{-3}) of the World Health Organization (WHO) [45]. The NO_2 hourly concentrations at the two regulatory traffic stations in Sofia (marked as MS-1 and MS-5 in Figure 2b) have

in 2023 maximum values of 147 μg m^{-3} and 116 μg m^{-3}, thus below 200 μg m^{-3}, the EU norm [34] and WHO guidance value [45]. The daily mean NO_2 concentrations at the two stations have values above the WHO guidance of 25 μg m^{-3} in more than 30% of the days in 2023 (respectively, 183 days and 118 days).

The mean annual PM_{10} concentrations are in the range of 23.7–31.4 μg m^{-3} (2022) and 19.4–27.5 μg m^{-3} (2023), also below the AAQD annual limit value (40 μg m^{-3}), but up to two times higher than the WHO guidance value (15 μg m^{-3}). The main problem is that, with high daily mean PM_{10} concentrations, especially in the winter period, the AAQD daily norm of 50 μg m^{-3} is often exceeded. For example, the number of days with daily mean PM_{10} concentrations above 50 μg m^{-3} was between 7 and 29 (2023) and between 11 and 47 (2022).

Previous air quality modelling results for Sofia [38,39,43,44] showed that the stations do not capture the high spatial variability of the pollutants. Although in these studies there are attempts to provide more detailed spatial resolution, they do not treat the effects of single buildings on the flow and concentration fields.

The main sources of pollutants in the city of Sofia are road transportation and residential heating. Road transportation was estimated to be responsible for 78.7% of NO_X emissions and 10.8% of PM_{10} emissions in 2018 [39].

Aiming at reducing emissions from road transportation, the European Union (EU) has introduced since the 1990s a series of regulations known as Euro standards (Euro 1 to Euro 6). The standards limit exhaust emissions from new petrol and diesel vehicles, referring to nitrogen oxides, particulate matter, carbon monoxide, hydrocarbons, and other pollutants. The pre-Euro standard cars are the most polluting, while each new standard imposes stricter limits, especially for diesel vehicles. Pre-Euro 5 diesel vehicles (produced before 2009) emit significantly more PM and NO_X emissions than those certified to newer standards.

The motorization rate for Sofia is one of the highest in Europe (663 cars per 1000 inhabitants in 2020), but the vehicles are old, with a mean age of 19 years (data provided by Sofia Municipality). In 2020, the vehicle fleet predominantly consisted of cars, representing approximately 80% of the total. Furthermore, over 70% of the cars were equipped with engines that did not meet the Euro 5 standard (Figure 4). Recent estimates related to the introduction of Low-Emission Zones (LEZs) in the city [43] show that about 78% of the cars using petrol have a standard below Euro 5, while more than 55% of the diesel cars have a standard below Euro 3 and Euro 4. The most polluting vehicles in Sofia use diesel fuel, contributing 74% of the total NO_X emissions and 86% of the total PM emissions from passenger cars in Sofia [44].

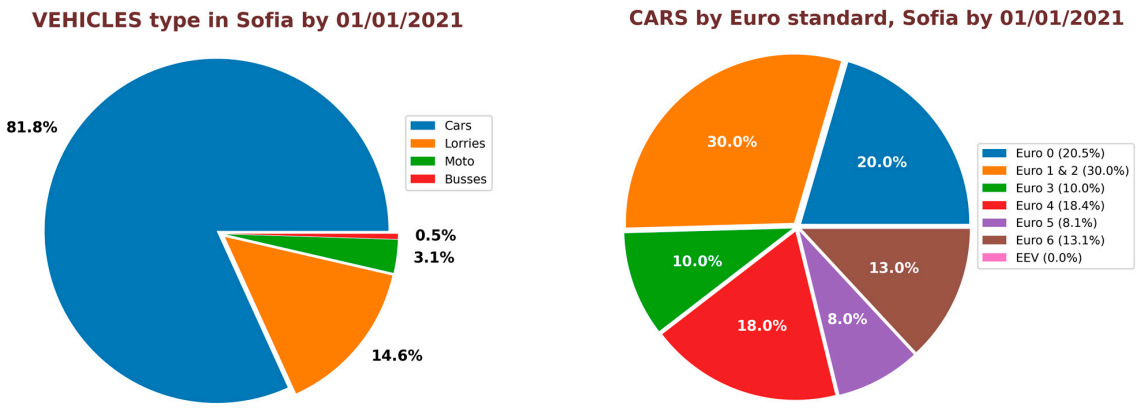

(**a**) (**b**)

Figure 4. (**a**) Vehicles type in Sofia up to 1 January 2021; (**b**) Cars by Euro standard, Sofia up to 1 January 2021.

This brief overview highlights that for fine-scale modelling of the dispersion of pollutants in Sofia, the system should be capable of treating built-up elements and low wind conditions.

2.2. GRAMM/GRAL Model System

This study employed the GRAMM/GRAL system (version 22.09), developed at the Technical University of Graz, Austria [18,31,32]. The system was initially created to address the issues caused by frequent stagnation episodes of atmospheric pollutants in the mountain valleys of Austria. Similar situations have also been observed in Bulgaria, particularly in some lowland regions, making this model pertinent for the city of Sofia.

GRAMM is a mesoscale prognostic non-hydrostatic model that calculates hourly steady-state wind fields over complex terrain [46]. It solves the conservation equations for mass, enthalpy, momentum, and humidity and considers the effects of the topography and the land use in the studied domain. The meteorological input consists of wind speed, wind direction, and atmospheric stability class. The flow field calculated by GRAMM is used as input to the second module of the system, GRAL.

GRAL is a microscale model that includes a CFD module for explicitly accounting for the effects of urban structures (e.g., buildings, tunnels, etc.) on the air flow and a Lagrangian particle dispersion module (LPDM) for the simulation of the transport and diffusion of pollutants [18]. The CFD module in GRAL solves the Navier–Stokes equations for incompressible flow, incorporating k-ε turbulence models to simulate the microscale turbulence characteristics. The high-resolution air flow provided by the CFD, and the emissions data are then used by LPDM to produce the concentration distribution. The dispersion model assumes that particles are transported by the mean wind field and dispersed by turbulence. It calculates the concentration of pollutants by solving the advection–diffusion equation, which includes terms for advection, turbulent diffusion, and gravitational settling. Chemical reactions are not treated.

A key feature of the GRAMM/GRAL system is the classification of weather situations based on wind speed, direction, and atmospheric stability. Atmospheric stability is categorised using the Pasquill-Gifford (PG) 7-level scheme, which classifies the stability from very unstable to very stable conditions [47,48]. By default, wind direction is divided into 36 sectors of 10 degrees each and wind speed into five classes, creating a matrix of 1260 distinct meteorological situations.

The primary reason for this categorization is to facilitate the 'match to observation' approach employed by the GRAMM/GRAL system. By pre-computing wind fields for these discrete intervals, the system can significantly reduce computational demands during operational forecasting or regulatory assessments. When real-time meteorological data are available, the GRAL model matches the observed conditions to the pre-calculated wind fields, thereby eliminating the need for repetitive calculations of the three-dimensional wind field. This approach streamlines the process, focusing computational resources on pollutant dispersion calculations. The efficiency and practicality of this method make it particularly advantageous for regulatory applications and air pollution forecasting, ensuring timely and accurate assessments [33].

In summary, the GRAMM/GRAL system leverages the strengths of both mesoscale and microscale modelling to provide a comprehensive framework for air pollutant dispersion simulations. By integrating detailed topographical influences and urban infrastructure interactions, the system offers robust capabilities for addressing complex dispersion scenarios in various environmental settings. GRAL is extensively used for regulatory purposes and research in Austria [33,49], but also in other European countries [50,51]

2.3. Modelling Set-Up

2.3.1. Modelling Domain

The study area is located within the residential district of Mladost-1 in Sofia, Bulgaria. It encompasses an eight-story block of flats, a nearby kindergarten, and a busy roadway in close proximity (Figure 5). The roadway (Alexander Malinov Boulevard) is two-directional, with three traffic lanes in each direction. The boulevard serves as a principal thoroughfare for the residential district of Mladost (with a population of approximately 116,000), facilitating connectivity between this area and the city centre. Additionally, it represents

a significant artery linking the Sofia Ring Road to the airport and major eastward routes within the city. The boulevard is also utilised by public transport buses.

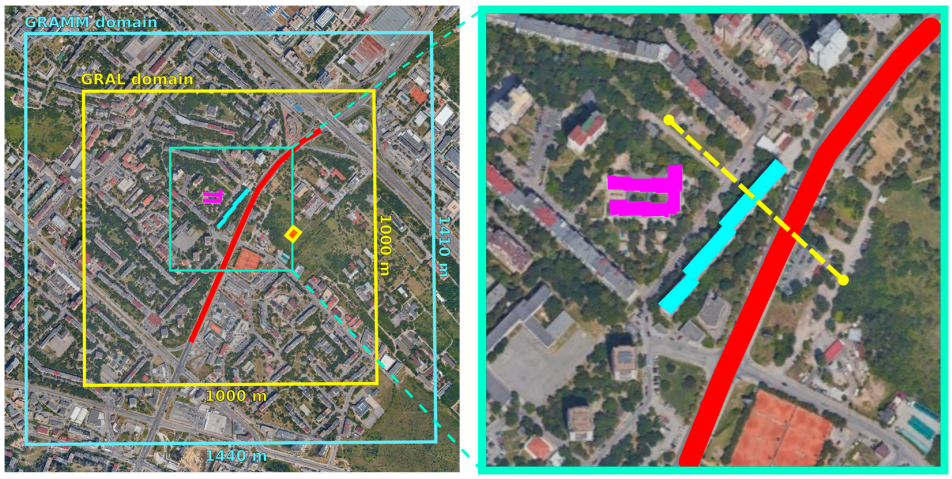

(**a**) (**b**)

Figure 5. (**a**) GRAMM/GRAL domains and elements in consideration: Alexander Malinov Boulevard (red line), the block of flats (cyan), and the kindergarten (magenta); the yellow box marks the location of standard meteorological measurements at NIMH; (**b**) zoom on the GRAL domain with the mentioned elements. The yellow dashed line marks the location for vertical cross-section in analysing concentration distribution.

The modelling domains have horizontal dimensions of approximately 1400 m (for GRAMM) and 1000 m (for GRAL). The vertical extent is up to 1402 m a.g.l. for GRAMM and up to 170 m a.g.l. for GRAL. The dimensions of the block of flats are (L × W × H) 163 × 11 × 25 m, and the length of the boulevard in the GRAL domain is 880 m, with a width of 20 m. The blockhouse makes an angle of 18 degrees with the boulevard.

Both GRAMM and GRAL adopt a calculation mesh that is regular in the horizontal direction (respectively 30 and 2 m) and stretching in the vertical direction, with intervals near the ground of about 10 m for GRAMM and 2 m for GRAL. The specifics of the domains describing the type of calculation mesh, resolution, and number of cells are summarised in Table 1.

Table 1. GRAMM and GRAL calculation mesh configuration.

Parameter	GRAMM	GRAL
Terrain elevation range, m	565–611	Inherited from GRAMM
Domain size (x, y), m	1440 ⊚ 1410	1000 ⊚ 1000
Horizontal cell size, m	30	2
Number of cells in the E-W direction	48	500
Number of cells in the N-S direction	47	500
Number of vertical levels	12	50
Thickness of the first level, m	10	2
Vertical stretching factor	1.4	1.02

The definition of the simulation grid is critical in CFD modelling, as this directly influences the accuracy and computational efficiency of the simulations. GRAL uses a structured Cartesian grid system for the finite difference method solver of the governing equations. Other CFD codes, such as OpenFOAM, employ unstructured (irregular) grid system, which can be adapted to complex geometries for a more detailed representation of urban elements [52]. A computational mesh that supports various types of cells in OpenFoam (tetrahedral, hexahedral, etc.) is also linked to another solver of the governing

equations, the finite volume method. The flexibility that such a type of discretisation offers is higher and requires more sophisticated meshing techniques and greater computational resources. GRAL, instead, is computationally efficient and advantageous for long-term simulations in cases of limited computational resources. The structured grid system in GRAL allows for efficient numerical calculations and is well-suited for the 'match-to-observation' approach of the system GRAMM/GRAL.

The boulevard is represented as a line source with an emission rate of 100 Lagrangian particles per second. This particle quantity is derived from the recommendations in the GRAL manual [53]. It can be observed that, as the number of Lagrangian particles increases, the concentration fields become more smooth (statistical errors are reduced with an increasing number of particles). Typical values are between 25 (for areas smaller than 250×250 m^2) and 1000 (for areas larger than 20×20 km^2 and numerous sources). In the case of high-stack sources or a limited number of weather situations, it is recommended to use a significantly higher number of particles. In the majority of cases, where there are few sources and areas smaller than 1 km^2, 100 particles per second is a suitable choice.

2.3.2. Calculation of Traffic Emissions

In this study, the dispersion of NO_X as a pollutant that is emitted in greater quantities from diesel vehicles was modelled and discussed.

Prior to estimating the emissions for this study, the traffic flow was evaluated based on the results of vehicle counting conducted over a number of days. The analysis of vehicles was organised in the framework of a project about mobility and transport in the city [54]. The counting was carried out at 15-min intervals between 2 May and 8 May 2023. Three categories of vehicles were considered during the counting campaign: cars, commercial vehicles (trucks), and buses. During the aforementioned period, three consecutive days were days off—two were over the weekend, while the third was a public holiday. The mean traffic flow, for both working days and holidays, is presented in Figure 6.

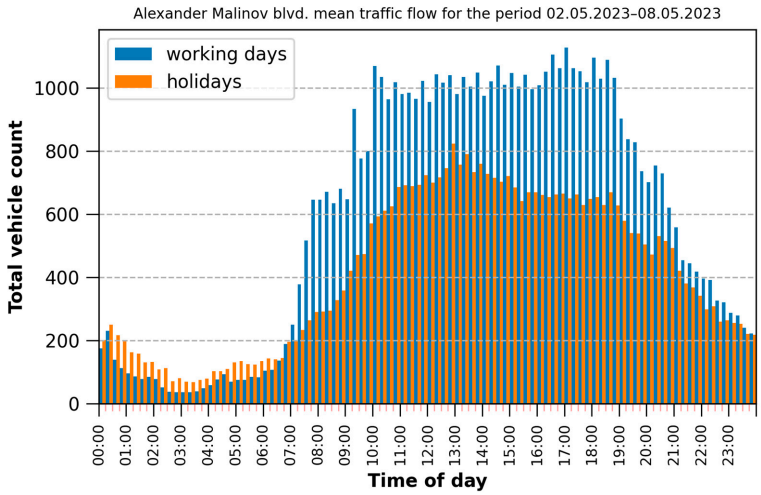

Figure 6. Average traffic flow around the clock on Alexander Malinov Boulevard—the blue bars show the traffic on weekdays and the orange bars show the traffic on holidays.

As illustrated in Figure 6, the workday traffic does not exhibit distinct peak hours. Instead, the period spanning from 10:00 to 18:45 local time represents a plateau with a mean traffic flow of 1030 vehicles per 15 min (4120 vehicles per hour). For comparison, the mean flow for the entire 24-h period is 600 vehicles per 15 min (2400 vehicles per hour). The total vehicle count per working day is 57,593, of which 541 are public transport buses.

The mean number of vehicles in a working day and their distribution by type are summarised in Table 2. The data presented there show both the mean total number of vehicles for the day and for the hours between 10:00 and 18:45 local time.

Table 2. Mean traffic distribution by vehicle type for the working days on Alexander Malinov Blvd. LCV stands for light commercial vehicles, MCV for medium commercial vehicles, and HCV for heavy commercial vehicles.

Vehicle Type	Total Traffic for 24 h	Mean Hourly Traffic for 24 h	Total Traffic for Peak Hours	Mean Hourly Peak Traffic
Cars (petrol)	21,376	890	13,773	1574
Cars (diesel)	29,070	1211	18,726	2140
Buses	541	22	313	35
LCV, MCV, and HCV	6606	275	4260	486
Total	57,593	2398	37,072	4235

Some assumptions have been made regarding the vehicle distribution shown in Table 2. Firstly, it is assumed that there are no electrical, hybrid, or liquefied petroleum gas (LPG) vehicles passing through the point of counting. Secondly, the share of diesel and petrol cars was estimated based on the national statistical data for the transport fleet by 1 January 2024. The data, provided by the Ministry of Interior, are available in the open data portal [55]. The numbers for vehicles by fuel type were used to estimate the ratio of cars using petrol and diesel. As an approximation, this ratio was then applied to split the counted cars by fuel type. Lastly, it was assumed that all commercial vehicles and buses consume diesel fuel. Therefore, in determining the emissions, the commercial vehicles and the buses were combined into one category: 'trucks and buses'. The mean fuel consumption and mean emission rates of this category were calculated based on the ratio between the numbers of these two vehicle types.

Based on the data presented so far, the emission rates (kg h^{-1} km^{-1}) of carbon monoxide (CO), non-methane volatile organic compounds (NMVOC), particulate matter (PM), black carbon (BC), and NO_X were calculated using the formulation and emission factors from the Tier 1 method from the EMEP/EEA (European Monitoring and Evaluation Programme/European Environment Agency) air pollutant emission inventory guidebook [56]. More information about the calculated total emissions (kg h^{-1} km^{-1}) for dispersion simulations with GRAL is presented in Table 3.

Table 3. Mean traffic flow of vehicles (vehicles per hour) by category type passing through the road section of interest for the period 10:00–18:45, and emission rates of CO, NMVOC, NO_X, PM, and BC (kg h^{-1} km^{-1}) as used by GRAL.

Vehicles		Emission Rate (kg h^{-1} km^{-1})				
Type	Count per Hour (Peak Mean)	CO	NMVOC	NO_X	PM	BC
Cars (petrol)	1574	7.2514	0.8604	0.7474	0.0026	0.0003
Cars (diesel)	2140	0.3322	0.0698	1.2930	0.1097	0.0626
Buses	35	0.0224	0.0049	0.0549	0.0043	0.0023
Trucks	486	0.3052	0.0660	0.0581	0.7474	0.0310
Total	4235	7.9112	1.0011	2.1535	0.8640	0.0962

2.3.3. Numerical Experiments and Meteorological Set-Up

Two types of numerical experiments with GRAMM/GRAL were considered: 'test cases' and 'real cases.' 'Test cases' refer to hypothetical meteorological conditions when combinations of wind and atmospheric stability are pre-defined. Here, we focused only on the combinations for which the highest concentrations of pollutants around the block of flats might be expected. The emissions for the 'test cases' were chosen to correspond to the highest traffic intensity (the interval between 10:00 and 18:45) in order to capture the greatest impact of the emissions in the studied domain. The second type of simulation ('real

case') refers to a real meteorological situation during the period between 2 May and 8 May 2023. The emission input in this case corresponds to the counted vehicles on the boulevard.

Meteorological Set-Up for the 'Test Cases'

The selected meteorological conditions are guided by the geometry and the orientation of the building of interest (southwest-northeast direction), as shown in Figure 4. Thus, four different wind directions of the approaching flow were selected: along the length of (parallel to) the building (southwest and northeast winds), and perpendicular to the building (northwest and southeast winds). The last cases are of particular interest, as development of recirculation flows on the leeward side of buildings, trapping of pollutants, and elevated concentrations might be expected [57–59].

For each of the aforementioned wind directions, as a sensitivity test, simulations were conducted under different wind intensities at wind speeds of 3 and 7 m s^{-1}. Calm conditions were considered in a separate case. The stability classes applied were 1, 4, and 7, which correspond to strong unstable, neutral, and strong stable temperature stratification, respectively. A summary of the test case set-up is provided in Table 4.

Table 4. Summary of the test case set-up.

Test Case	Wind Direction	Wind Speed	PG Stability Class
Case 1	---	0 m s^{-1}	1, 4, and 7
Case 2	NW (315°)	3 m s^{-1}, 7 m s^{-1}	1, 4, and 7
Case 3	SE (135°)	3 m s^{-1}, 7 m s^{-1}	1, 4, and 7
Case 4	NE (45°)	3 m s^{-1}, 7 m s^{-1}	1, 4, and 7
Case 5	SW (225°)	3 m s^{-1}, 7 m s^{-1}	1, 4, and 7

Meteorological Set-Up for the 'Real Case'

Regarding the real meteorological observations, we looked at the data from the NIMH synoptic station (marked in Figure 5a). From 2 May to 8 May 2023, the observed wind speed was below 4 m s^{-1}, with a predominant wind direction from the southeast (Figure 7a). This makes the real case similar to that of 'Case 3' for the majority of time intervals. To estimate the stability class, we used an analysis of observed wind, temperature, cloud cover, solar radiation, and radio sounding data at this site. The estimated stability class distribution (Figure 7b) indicates the prevalence of neutral and, to a lesser extent, stable conditions.

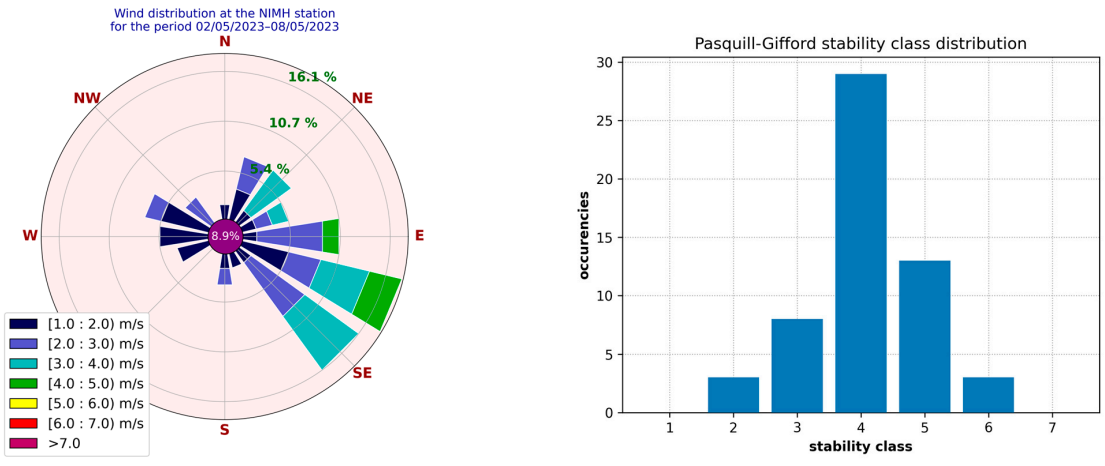

(**a**) (**b**)

Figure 7. (**a**) Wind rose observed at NIMH meteorological stations for the period 2 May 2023–8 May 2023; (**b**) Estimated distribution of stability classes for the period as prepared for GRAMM/GRAL.

3. Results

The modelling results are presented and discussed in terms of the horizontal and vertical distribution of hourly mean NO_X concentrations and maximum concentrations simulated in the domain of interest. The spatial distribution is discussed more in depth for the most interesting test cases with calm conditions and a flow perpendicular to the boulevard ('Case 1' and 'Case 2'), as well as for the real case. For the latter case, comparisons to observations at the nearby air quality station are discussed.

3.1. Pollution Distribution Sensitivity to 'Test Cases' Meteorological Setup

3.1.1. 'Case 1' Results

Figure 8 displays the simulated horizontal fields of hourly mean nitrogen oxide concentrations at a height of 2 m, along with the corresponding vertical fields at the selected cross-sections, under calm conditions for stability classes: 1 (strongly unstable), 4 (neutral), and 7 (strongly stable).

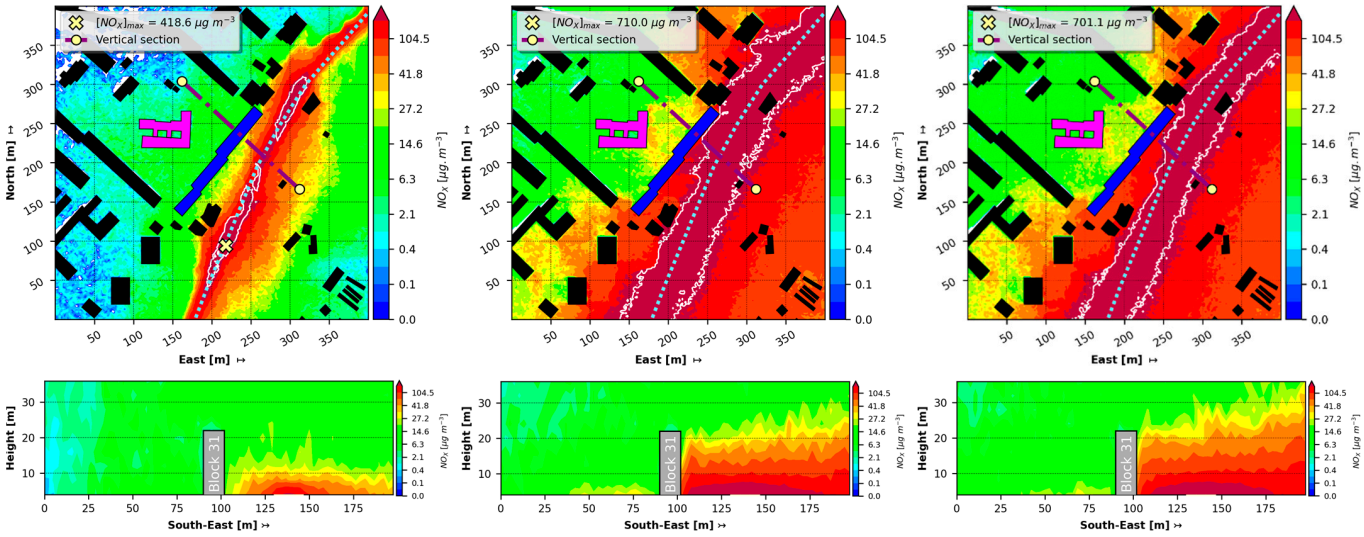

(**a**) (**b**) (**c**)

Figure 8. Fields of NO_X 1-h averaged concentrations (μ gm^{-3}) for 'Case 1' test case: calm and SC = 1 (**a**), SC = 4 (**b**), and SC = 7 (**c**); top at a height of 2 m; bottom along the vertical cross-section marked by a dashed line. White isolines enclose the zones with $NO_X \geq 200$ μ gm^{-3}: apartment building (blue), kindergarten (magenta).

The dispersion in the vertical directions is more enhanced in the modelling results for strong instability (Figure 8a). With regard to air pollution from sources located close to the ground (as traffic emissions), the conditions of strong instability are considered favourable, as the pollutants are more easily dispersed far from the source and distributed in the greater volume of a well-developed surface layer.

In contrast, under conditions of neutral and stable temperature stratification, pollutants are retained close to the ground surface, resulting in their accumulation and increased concentrations (Figure 8b,c). The areas enclosed by white isolines ($NO_X \geq 200$ μg m^{-3}) indicate a possible exceedance of the hourly limit value for NO_2 concentrations (200 μg m^{-3} AAQD [34]). As to be expected, the maximum concentrations are near the road (about 700 μg m^{-3}). Pedestrians walking along the boulevard might be negatively impacted by high surface-level concentrations. In the model domain, the horizontal gradients are very steep due to the presence of buildings.

The apartment block appears to act as an effective barrier against NO_X penetration into the area where the kindergarten is located, at least for the steady-state time interval of one hour. The spatial pollutant distribution for stability classes 4 and 7 shows smaller

differences. This indicates that the modelled mixing in the surface layer has similar values under neutral and stable conditions at this scale. As previously stated in Section 2.3.3, conditions for either strongly unstable (daytime) or strongly stable (night-time) stratification may be present for wind speeds less than 2–3 m s^{-1}. This is treated as a separate case in the following section.

3.1.2. 'Case 2' Results

In this case, the approaching flow is from the northwest (315°), and the road (Alexander Malinov Boulevard) is on the downwind side of the apartment block (Figure 9).

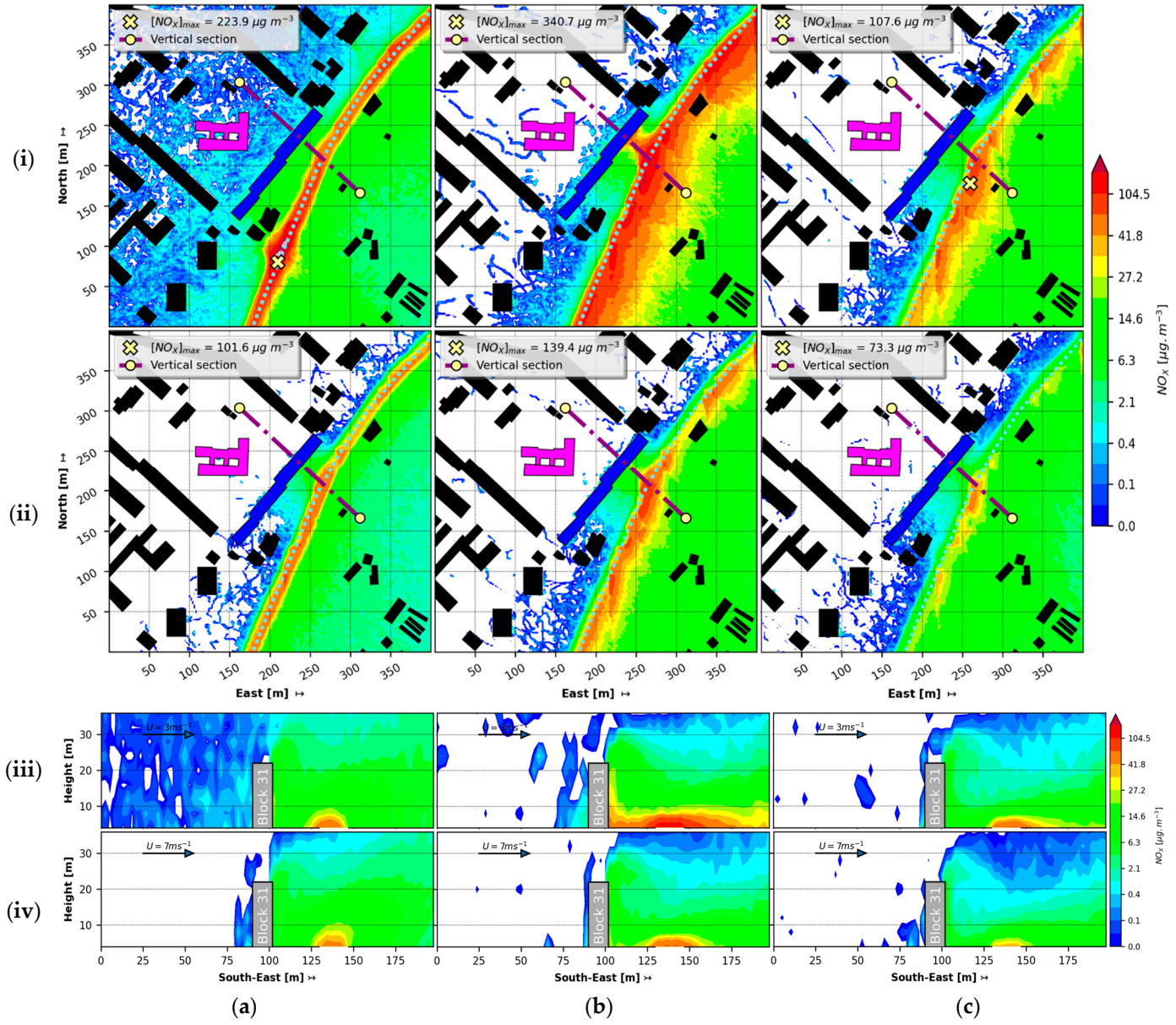

Figure 9. Fields of NO_X 1-h averaged concentration (μg m^{-3}) for 'Case 2' test case: NW wind with speeds of 3 m s^{-1} and 7 m s^{-1} and SC = 1 (**a**), SC = 4 (**b**), and SC = 7 (**c**); horizontal distribution at 2 m: (**i**,**ii**); vertical cross-section along the dashed line: (**iii**,**iv**); apartment building (blue), kindergarten (magenta); dotted line: axis of the road. The 'X' sign marks the spot with the highest concentration. If the sign is missing on the map, the highest concentration is outside of the shown area but within the model domain.

The pollutant vertical distribution is linked to the modifications made to the airflow by the building.

The airflow around the building is influenced in such way that a recirculation zone on the leeward side is developed, and the wind shifts in an almost opposite direction compared to the approach flow direction (Figure 10). As can be seen in Figure 9 ((a), (b), (c)–(i) and (ii)), where Alexander Malinov Boulevard is close to the building, the pollutant enters this zone and accumulates. As a result, the concentration there increases significantly.

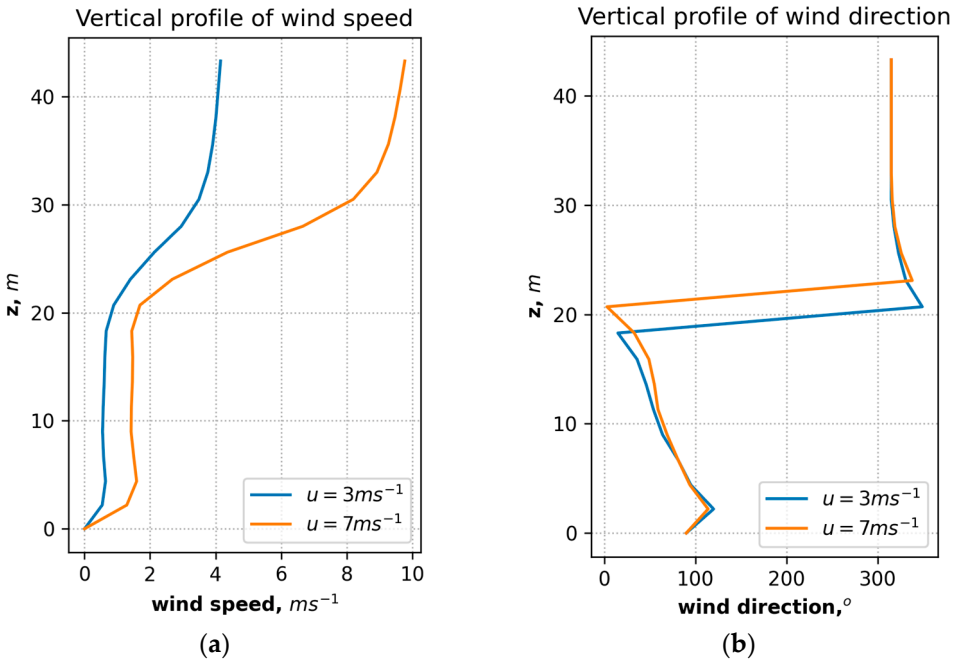

Figure 10. Modelled by GRAL vertical profiles of wind speed (m s^{-1}) (**a**) and wind direction (**b**) (degrees) in the middle point lying on the vertical section between the apartment block and Alexander Malinov Boulevard, for 'Case 2' (northwestern wind). The wind gradually shifts to reach a direction at a height of approximately 3 metres that is opposite to that of the approaching flow.

Again, as in the case of calm weather ('Case 1'), for unstable conditions, the resulting (modified) air flow provides a better dispersion of NO_X in the vertical direction, which reduces the otherwise high concentrations at the building wall observed in the case of a neutral and stable stratified surface layer. However, as can be seen, this is at the expense of slightly increased pollutant concentrations on the windward side of the building.

3.1.3. Stability Class Modifications by GRAMM

It is important to note that not all combinations of stability class and wind speed are feasible in real-world scenarios. For instance, in calm conditions, any stability class can be realized. As wind speed increases, there comes a point where dynamically generated turbulence begins to outweigh thermally generated turbulence. At the wind speed of 7 m s^{-1} used in this study, mixing in both horizontal and vertical directions is well pronounced, resulting in temperature homogenization throughout the roughness sublayer in the urban canopy. These conditions permit only neutral temperature stratification (stability class 4). The meteorological input to GRAMM refers to stability class, wind speed, and direction that should be representative of the modelled domain. GRAMM calculates, along with the flow field, several other parameters related to turbulence and dispersion simulations (friction velocity scale, planetary boundary layer height, and Monin–Obukhov length). These parameters are the basis for a GRAMM estimated stability class that may differ from the original user input.

A test was conducted to ascertain the impact of the GRAMM stability class on the user input model. This was performed for Case 2, with all possible combinations of wind speeds and stability classes defined for this case.

The simulated stability class has varying values, as shown in Figure 11. Each row in the figure refers to results by input wind speed (calm, 3 m s^{-1} and 7 m s^{-1}) and each column refers to results by input stability classes (SC = 1, 4, and 7). Examination of the first row, which corresponds to calm conditions, shows that GRAMM does not modify the input conditions in the domain. For wind speeds of 3 m s^{-1} and 7 m s^{-1} (the second and third rows in Figure 11), the input stability class in the domain was modified by GRAMM. For input SC = 1 (strongly unstable), the approaching flow with a speed of 3 m s^{-1} was slightly modified by GRAMM, while for the case with wind speed of 7 m s^{-1} the modification was more pronounced, resulting in SC = 3–4 in some limited zones. For SC = 4 (neutral), no modifications took place, while for SC = 7, they are considerable. It should be noted here that the outermost frame of the GRAMM domain in all of the instances in Figure 11 represents the stability class boundary conditions, which remain constant throughout the calculation of the fields. The frame also shows what the initial stability class was in the entire domain.

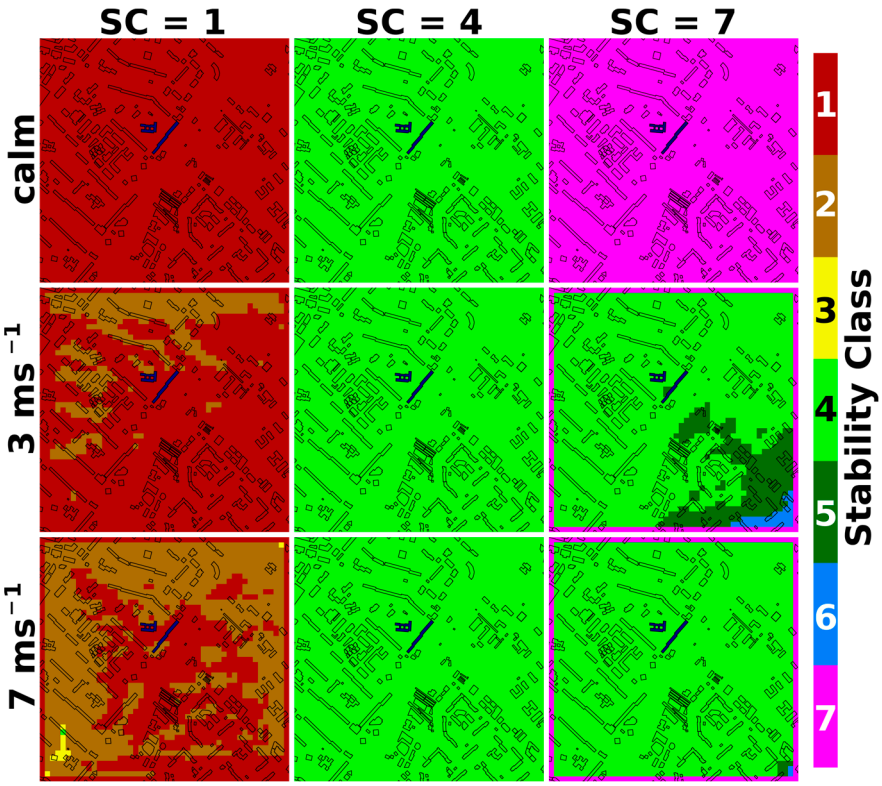

Figure 11. Sensitivity of GRAMM to wind speed—stability class consistency. The buildings of interest are in dark blue.

3.1.4. Other Cases: 'Case 3', 'Case 4', and 'Case 5'

In 'Case 3', regarding SC = 1 (strong instability), a relatively small part of the pollutant enters the recirculation zone on the lee side of the block, as the main part of the NO_X is entrained by convection and transported to a greater height. In the case of neutral or stable stratification (SC = 4, 7), higher concentrations are observed both on the windward side—near the wall that is directly affected by the pollutant plume—and on the leeward side. At a wind speed of 3 m s^{-1}, the maximum modelled concentration for SC = 1 is 181.2 μg m^{-3}, for SC = 4, it is 216.8 μg m^{-3}, and for SC = 7, it is 106.3 μg m^{-3}. For wind speeds of 7 m s^{-1}, the corresponding concentrations are 81.3, 91.3, and 61.6 μg m^{-3}.

In 'Case 4' and 'Case 5' (wind directions parallel to the building), the distribution of pollutant concentrations is primarily influenced by the geometrical position of the boulevard and the block (they are not ideally parallel). This leads to an asymmetry in the pollutant distribution when looking at the residential area, located northwest of the building. When the wind flow is from the northeast, NO_X penetrates the inner residential area to a greater extent than when the wind blows from the southwest. In the latter case, the building functions as a deviating obstacle and leads to pollutant transport along the boulevard towards the northeast. In both cases, however, the plume has a direct impact on the wall of the building facing the boulevard.

The modelled maximum concentrations for all the cases mentioned so far are summarised in Table 5.

Table 5. Modelled maximum concentrations of NO_X ($\mu g\ m^{-3}$) within the GRAL domain for all cases.

Stability Class	Wind Direction	NW (315°) ('Case 2')		SE (135°) ('Case 3')		SW (225°) ('Case 5')		NE (45°) ('Case 4')		Calm Conditions ('Case 1')
	Wind Speed	3 m s^{-1}	7 m s^{-1}	3 m s^{-1}	7 m s^{-1}	3 m s^{-1}	7 m s^{-1}	3 m s^{-1}	7 m s^{-1}	
Strongly unstable (SC = 1)		223.9	101.6	181.2	81.3	244.0	90.4	168.8	75.4	418.6
Neutral (SC = 4)		340.7	139.4	216.8	91.3	217.6	256.8	206.3	186.3	710.0
Strongly stable (SC = 7)		107.6	73.3	106.3	61.6	216.2	177.8	241.4	309.1	701.1

The highest values for the maximum NO_X concentrations were modelled for the calm case, as expected. As the wind speed increases, the maximum concentrations generally decrease, but this behaviour is influenced by the direction of the approaching flow. For flow perpendicular to the building, the wind speed of 7 m s^{-1} resulted in a maximum NO_X concentration lower by a factor of about 2 compared to the wind speed of 3 m s^{-1}. For flow parallel to the building, the effect of increased wind speed was more influenced by the stability class. For certain combinations of wind direction and neutral or stable atmosphere, the highest values of maximum NO_X concentrations were modelled for the higher wind speed.

Note should be taken here that the values of the maximum concentrations presented in Table 4 should not imply any proportionality with the corresponding fields they were extracted from. In all cases where obstacles are involved, the locations of maximum concentration points are subject to the complex wind field configurations due to the complex geometry of the urban environment.

3.2. Pollution Distribution in Real Meteorological Conditions

This section presents the results as mean, maximum, and daily maximum NO_X concentration fields for the entire period between 2 May and 8 May 2023. The meteorological data provided by the synoptic station at NIMH are updated every three hours. We consider this time interval further because, in many cities in Bulgaria, the meteorological information is only provided by this type of station. The traffic data were calculated in accordance with the aforementioned settings. The distinction between this case and the previous cases lies in the fact that, in this case, time variations of both meteorological data and traffic emissions are considered. The NO_X concentration fields are shown as mean, daily maximum, and concentrations of maximum value at each grid node during the entire period (Figure 12). The NO_X concentrations were measured at the MS-1 site, which falls within the GRAL domain.

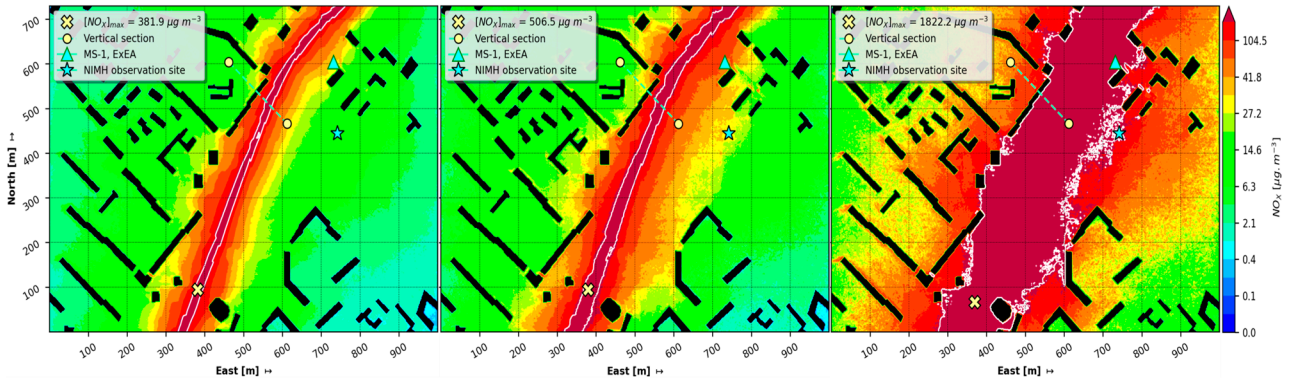

(**a**) (**b**) (**c**)

Figure 12. Modelled NO_X spatial distribution for the period between 2 May and 8 May 2023, utilising data from meteorological observations: (**a**) Mean concentrations; (**b**) Daily maximum concentrations; (**c**) Concentrations of maximum value at each grid node during the entire period. The MS-1 station is identified by a cyan triangle, while the NIMH observation site is marked by a cyan star.

Regardless of the manner in which the concentration fields are analysed, whether as an average over the entire period, the daily maximum, or the absolute maximum, it can be observed that there is an area along the road where the concentration levels are significantly higher. During the period of interest, the approaching flow was predominantly from the east by southeast (Figure 7a), which is a direction almost perpendicular to the main building. Figure 11 indicates that the block of apartments acts as a barrier against the penetration of pollutants into the inner residential area. The configuration of the two adjacent residential buildings at right angles to the block serves to further restrict the transport of NO_X in the vicinity of the kindergarten. The spatial distribution is characterised by very steep gradients (Figure 12a,b), while the absolute maximum concentrations (Figure 12c) follow a rather homogeneous distribution.

The modelled NO_X concentrations and wind speed were compared to the observed values at the MS-1 measuring site. The comparison between the modelled and measured NO_X concentrations was made using the recommended statistical performance measures for such cases: the normalised mean square error (NMSE), the fractional bias (FB), the correlation coefficient (R), the fraction of predictions within a factor of two observations (FAC2), and the fraction of predictions within a factor of five observations (FAC5) (Appendix A, Equations (A1)–(A4)). The results from the comparison are summarised in Table 6.

Table 6. Values of the statistical performance measures (SPMs) used to compare modelled NO_X concentrations against the observed NO_X concentrations at the ExEA MS-1 station in the time interval 2–8 May 2023.

FB	NMSE	R	FAC2 (%)	FAC5 (%)
−0.003	3.652	0.069	21.4	57.1

The mean modelled and mean measured concentrations at station MS-1 for the period under consideration were 16.95 μg m^{-3} and 16.89 μg m^{-3}, respectively. These values are almost identical and are well reflected in the FB value. However, the other statistical parameters show a large scatter, indicating that there are significant differences between the modelled and measured concentrations in general. There could be several reasons for these results. Firstly, the present study considers only one line source, Alexander Malinov Boulevard, but there are other pollution sources in the vicinity of the monitoring site, one of which contributes significantly, especially when the wind direction is from north and northeast—Tsarigradsko Shose Boulevard. Secondly, no background concentrations of NO_X were used as input. Thirdly, there is a difference between the modelled and measured

wind at the observation point. The measured wind speed values are significantly higher than the modelled values (Figure 13). Upon examination of Figure 13b, it becomes evident that there are discernible patterns in the relationship between the modelled wind speed and modelled NO_X concentrations. The presence of high peaks in the modelled concentrations at the observation point is observed at times of very light winds or when there is no wind. Conversely, during the initial period (between 2:00 on the 5 May and 14:00 on the 6 May), modelled concentration values were observed to be almost zero, which can be attributed to the prevalence of a south-easterly component in the wind direction, effectively transporting the pollutants emitted by the source away from the monitoring site MS-1.

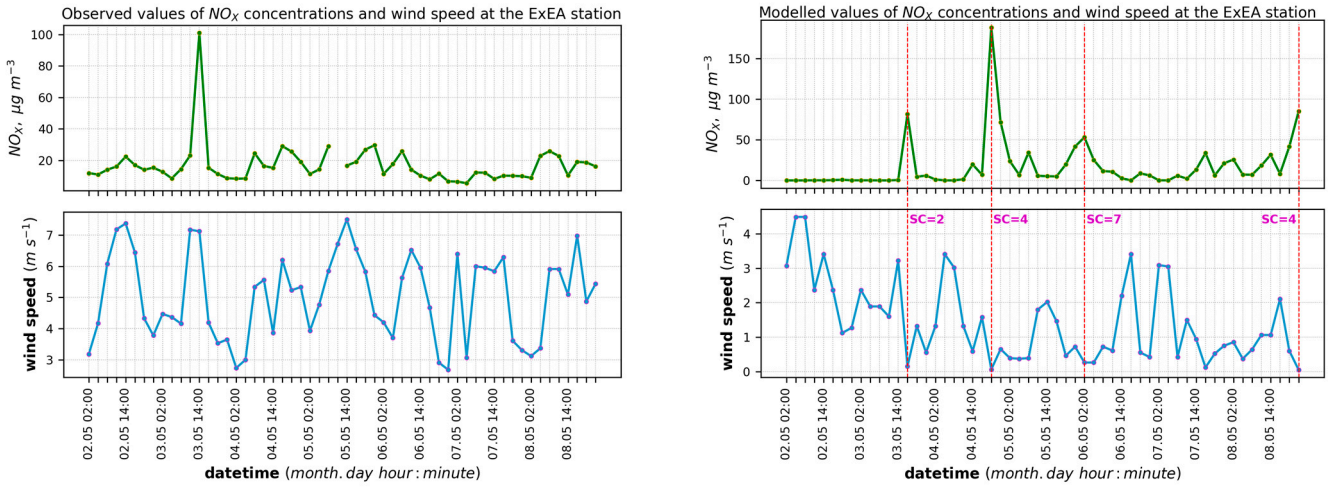

(**a**) (**b**)

Figure 13. Observed values of NO_X concentrations and wind speed at the ExEA station (**a**) and modelled values of NO_X concentrations and wind speed at the ExEA station for the period 2 May 2023–8 May 2023 (**b**).

4. Discussion

The air quality in the city of Sofia is monitored at five regulatory stations, which limits the scope of the data available for attaining a comprehensive city-wide spatial resolution of air pollutant concentrations. Modelling applications involving dispersion codes [38,39,60,61] or machine learning methods [62] clearly highlight the non-homogeneity in the spatial distribution of NO_2 and PM_{10} concentrations in Sofia and hot spots not captured by the AQ regulatory network.

The modelling of air pollutant concentrations in Sofia does not currently account for the effects of buildings. To estimate the dispersion of pollutants in Sofia with high resolution, it is necessary to apply models that can handle building-resolved flows. This is an emerging issue for authorities engaged with air quality plans and programmes, as it requires the estimation of exposure estimates.

The dispersion of pollutants is significantly influenced by urban morphology. As a preliminary step in the application of high-resolution model simulations in Sofia, we have employed the system GRAMM/GRAL for a limited area of the city with a horizontal resolution of 30 m for GRAMM and 2 m for GRAL. The system was selected due to its capacity for long-term simulations at a relatively low computational cost. The simulations are focused on a small residential area where the main source of emissions is a heavy traffic boulevard. A sensitivity analysis was carried out to assess the effect of meteorological conditions expressed as wind speed, wind direction, and stability class on the spatial distribution of NO_X. The sensitivity test was performed using predefined and real meteorological data. The simulations were carried out considering only the traffic on the boulevard as a source of air pollution. No background concentrations were applied. The emissions from road

traffic were estimated with assumptions for vehicle type and fuel count for a period of a week.

The spatial distribution of the GRAMM/GRAL simulated concentrations with predefined meteorological input (test cases) indicates the presence of hot-spot areas, whose locations vary with respect to wind direction, wind speed, and stability class. In the case of flows perpendicular to the main building (from the northwest), the higher concentrations on the leeward side are associated with an air flow recirculation zone that extends up to a height of about 20 m. In such conditions, the pollutants emitted by the vehicles on the boulevard remain entrapped and have elevated values not only near the ground. The main residential area and the kindergarten, situated on the windward side, remain almost without negative impacts from the traffic on the boulevard. This situation changed for calm conditions when the highest concentrations in the domain of interest were simulated. For neutral and stable conditions, the pollution from the boulevard could penetrate into the residential area, especially in the zones to the edges of the main building. The wind speed is decisive for the decrease in the concentrations, but this would also depend on the wind direction. For flows perpendicular to the building, the increase in the wind speed from 3 to 7 m s^{-1} leads to a decrease in the value of the maximum concentration in the domain by a factor of two. In certain configurations of the layout of the road in relation to a residential building, even higher wind speeds (7 m s^{-1}) have been found to be insufficient to ventilate the area.

The simulation of a real case (over a period of a few days) with prevailing winds from southeastern directions highlights rather favourable conditions for the main residential area, as the highest concentrations in the domain are simulated along the boulevard. The comparison to data from a regulatory air quality station of traffic type indicates an underestimation of the wind speed and a factor of two for the NO_X concentrations of approximately 21%. Further analysis and more data are needed to understand the behaviour of the simulated concentrations, which show distinct peaks at intervals with no wind or very low wind speeds.

Key limiting factors in the application for the real case are the compilation of emissions from the transport with high resolution, in this case, for a segment of a boulevard during a specific period, and the meteorological input. We used data from the nearby synoptic station, but as it is also located in a built-up environment and is only one, its representativeness for the conditions of the approaching flow should be additionally evaluated. Moreover, removal processes in the model were not considered.

It is important to note that the GRAMM/GRAL modelling system also has its own limitations. Firstly, the simulation of meteorological conditions that change rapidly (e.g., sudden changes in wind direction as in the passage of a frontal system) is limited by the steady-state approximation. Nevertheless, for research purposes, it is possible to utilise GRAL with the transient mode enabled. In this instance, the recommended minimum dispersion time can be reduced to 300 s. Secondly, GRAL is not capable of handling chemical reactions. Pollutants are treated as chemically inert, and the formation of secondary particles is not considered. In order to estimate the concentration of the monitored pollutant NO_2, the calculated NO_X concentration is typically modified according to empirical relationships derived from observations at different sites and over several years [63].

Despite the above-mentioned drawbacks, the GRAMM/GRAL system is suitable for modelling to take into account the influence of urban morphology on pollutant dispersion at a relatively low computational cost. This makes the system attractive for high-resolution modelling of the spatial distribution of pollutants in Sofia, which is currently needed for tasks related to the introduction of Low-Emission Zones (LEZs) and their impact on the redistribution of pollutant emissions in the city centre or for operational air quality forecasts. These tasks require, however the provision of high-quality input data: emissions, building layout, city-scale (background) concentrations, and meteorological information at more locations. The next steps in this research will be efforts to link the system to a meteorological model operating for Sofia and the compilation of necessary input data.

5. Conclusions

The GRAMM/GRAL modelling system was employed to analyse the spatial distribution of pollutants in a residential area of Sofia with high resolution (2 m) and to consider the effects of buildings on the flow and dispersion of pollutants. As this is the first study for Sofia with air pollution obstacle-resolving simulations, a series of numerical experiments were conducted to highlight the impact of meteorological parameters (wind and atmospheric stability) on the spatial distribution of NOx concentrations. A single type of emission source was selected for analysis: road traffic on Alexander Malinov Boulevard in the vicinity of the Mladost 1 residential area. The focus was on the potential increase in concentrations near a block of flats situated in close proximity and nearly parallel to the boulevard.

The numerical experiments were designed to reflect typical city wind conditions, which are characterised by calm weather and winds that originate from directions aligned with the orientation of the Sofia Valley (nearly northwest-to-southeast). These prevailing wind directions correspond to flow perpendicular to the boulevard and the main building in question, with the leeward side potentially leading to the formation of a recirculation zone and the accumulation of pollutants. This phenomenon has been observed in numerous experimental and modelling studies, including those by Murakami and Li [57,64]. The results of the simulation for 'Case 2' indicate that the wind direction at the block's leeward side at a height of approximately 3 metres (z/H = 0.12) is opposite to the flow at roof height. Furthermore, a recirculation area with low winds is observed there, reaching a height of approximately 20 metres (z/H = 0.8).

Additionally, a real-case simulation was conducted, utilising GRAMM/GRAL with input data from the synoptic station situated at approximately 170 metres from the boulevard. This was for a period of a few days, during which the prevailing wind direction was from the southeast. This resulted in a nearly perpendicular flow to the building, with the boulevard on the windward side. In this case, the building acted as a barrier for the spread of traffic-emitted concentrations towards the residential area and the nearby kindergarten. Unfortunately, observational data in the domain of interest were available only at one point: the regulatory air quality station located approximately 70 m to the east of the boulevard. The comparison between modelled and observed hourly wind speeds and NO_X concentrations was analysed using some common statistical metrics.

Notwithstanding the existence of certain significant limitations pertaining to the numerical experiments, including the use of rough estimates for traffic emissions, meteorological input data at three time intervals for the simulated real case, and the failure to consider the removal process in the model, the results demonstrated that the concentration field is highly variable. It is possible that different zones with an accumulation of pollutants may emerge, depending on the meteorological conditions. The modelling system GRAMM/GRAL was able to reproduce the expected pattern in the spatial distribution of concentrations and to highlight that the kindergarten might also be impacted by elevated concentrations, despite its distance from the considered road emissions. This initial application of GRAMM/GRAL for the simulation of air pollution in Sofia indicated that the system is appropriate in terms of computer resources for long-term calculations aimed at emission scenario analysis for air quality improvements or assessment of population exposure. Nevertheless, in order to gain confidence in the modelling results, further applications and validation with observations would be necessary.

Author Contributions: Conceptualization, A.P. and E.G.; methodology, A.P.; formal analysis, A.P., E.G. and E.H.; investigation, A.P. and E.G.; resources, E.G. and E.H.; data curation, A.P. and E.G.; writing—original draft preparation, A.P. and E.G.; writing—review and editing, E.G. and A.P.; visualization, A.P.; supervision, E.G. and E.H. All authors have read and agreed to the published version of the manuscript.

Funding: This research received no external funding.

Institutional Review Board Statement: Not applicable.

Informed Consent Statement: Informed consent was obtained from all subjects involved in the study.

Data Availability Statement: The raw data supporting the conclusions of this article will be made available by the authors on request. The data are not publicly available due to privacy.

Conflicts of Interest: The authors declare no conflicts of interest.

Appendix A

Statistical performance measures used for the comparison of modelled concentrations against observed concentrations:

$$\text{NMSE} = \frac{\overline{(c_o - c_p)^2}}{\overline{c_o}\,\overline{c_p}} \tag{A1}$$

$$\text{FB} = \frac{\overline{c_o} - \overline{c_p}}{0.5\left(\overline{c_o} + \overline{c_p}\right)} \tag{A2}$$

$$R = \frac{\overline{\left(c_o - \overline{c}_o\right)\left(c_p - \overline{c}_p\right)}}{\sigma_{\text{co}}\sigma_{\text{cp}}} \tag{A3}$$

$$FACX : \frac{1}{X} \leq \frac{c_o}{c_p} \leq X \tag{A4}$$

Here, c_o are the measured concentrations, and c_p are the concentrations predicted by the model. The mean values of c_o and c_p are indicated by $\bar{c}_o$ and $\bar{c}_p$, respectively, while the standard deviations of c_o and c_p are represented by σ_{co} and σ_{cp}. FB (A2) is a measure of mean bias and indicates only systematic errors that result in an underestimation or overestimation of the simulated values in comparison to the measured ones. It is based on a linear scale, and the systematic bias refers to the arithmetical difference between c_o and c_p. The NMSE (A1) is a measure of scatter that reflects both systematic and random errors. The correlation coefficient R (A3) reflects only the linear relationship between the measured and predicted values but, despite being a necessary condition for a perfect model, it is not a sufficient condition since it is sensitive to extreme data pairs. The FAC2 and FAC5 measures (presented in a more general form as *FAC X* in (A4)) are the most straightforward, as they consider only pairs with a ratio between 0.5 and 2.0 (0.2 and 5.0 for FAC5). This condition ensures that FAC2 and FAC5 are not overly influenced by high and low outliers.

References

1. Gill, S.S.; Wu, H.; Patros, P.; Ottaviani, C.; Arora, P.; Pujol, V.C.; Haunschild, D.; Parlikad, A.K.; Cetinkaya, O.; Lutfiyya, H.; et al. Modern computing: Vision and challenges. *Telemat. Inform. Rep.* **2024**, *13*, 100116. [CrossRef]
2. Bauer, P.; Thorpe, A.; Brunet, G. The quiet revolution of numerical weather prediction. *Nature* **2015**, *525*, 47–55. [CrossRef]
3. Blocken, B. Computational Fluid Dynamics for urban physics: Importance, scales, possibilities, limitations and ten tips and tricks towards accurate and reliable simulations. *Build. Environ.* **2015**, *91*, 219–245. [CrossRef]
4. Bouris, D.; Triantafyllou, A.G.; Krestou, A.; Leivaditou, E.; Skordas, J.; Konstantinidis, E.; Kopanidis, A.; Wang, Q. Urban-Scale Computational Fluid Dynamics Simulations with Boundary Conditions from Similarity Theory and a Mesoscale Model. *Energies* **2021**, *14*, 5624. [CrossRef]
5. Blocken, B.; Tominaga, Y.; Stathopoulos, T. CFD simulation of micro-scale pollutant dispersion in the built environment. *Build. Environ.* **2013**, *64*, 225–230. [CrossRef]
6. Lateb, M.; Meroney, R.N.; Yataghene, M.; Fellouah, H.; Saleh, F.; Boufadel, M.C. On the use of numerical modelling for near-field pollutant dispersion in urban environments. A review. *Environ. Pollut.* **2016**, *208*, 271–283. [CrossRef]
7. Li, Z.; Ming, T.; Liu, S.; Peng, C.; Richter, R.; Li, W.; Zhang, H.; Wen, C.Y. Review on pollutant dispersion in urban areas-part A: Effects of mechanical factors and urban morphology. *Build. Environ.* **2021**, *190*, 107534. [CrossRef]
8. Coceal, O.; Goulart, E.V.; Branford, S.; Thomas, T.G.; Belcher, S.E. Flow structure and near-field dispersion in arrays of building-like obstacles. *J. Wind Eng. Ind. Aerodyn.* **2014**, *125*, 52–68. [CrossRef]
9. Di Sabatino, S.; Buccolieri, R.; Salizzoni, P. Recent advancements in numerical modelling of flow and dispersion in urban areas: A short review. *Int. J. Environ. Pollut.* **2013**, *52*, 172–191. [CrossRef]
10. Bellasio, R. Modelling traffic air pollution in road tunnels. *Atmos. Environ.* **1997**, *31*, 1539–1551. [CrossRef]
11. Berkowicz, R. OSPM—A Parameterised Street Pollution Model. *Environ. Monit. Assess.* **2000**, *65*, 323–331. [CrossRef]

12. Vardoulakis, S.; Fisher, B.E.A.; Pericleous, K.; Gonzalez-Flesca, N. Modelling air quality in street canyons: A review. *Atmos. Environ.* **2003**, *37*, 155–182. [CrossRef]
13. Fu, X.; Liu, J.; Ban-Weiss, G.A.; Zhang, J.; Huang, X.; Ouyang, B.; Popoola, O.; Tao, S. Effects of canyon geometry on the distribution of traffic-related air pollution in a large urban area: Implications of a multi-canyon air pollution dispersion model. *Atmos. Environ.* **2017**, *165*, 111–121. [CrossRef]
14. Zhang, Y.; Ye, X.; Wang, S.; He, X.; Dong, L.; Zhang, N.; Wang, H.; Wang, Z.; Ma, Y.; Wang, L.; et al. Large-eddy simulation of traffic-related air pollution at a very high resolution in a mega-city: Evaluation against mobile sensors and insights for influencing factors. *Atmos. Chem. Phys.* **2021**, *21*, 2917–2929. [CrossRef]
15. Berkowicz, R.; Hertel, O.; Larsen, S.E.; Sørensen, N.N.; Nielsen, M. *Modelling Traffic Pollution in Streets*; National Environmental Research Institute: Roskilde, Denmark, 1997.
16. Kakosimos, K.E.; Hertel, O.; Ketzel, M.; Berkowicz, R. Operational Street Pollution Model (OSPM)—a review of performed application and validation studies, and future prospects. *Environ. Chem.* **2010**, *7*, 485–503. [CrossRef]
17. Stocker, J.; Hood, C.; Carruthers, D.; McHugh, C. ADMS-Urban: Developments in modelling dispersion from the city scale to the local scale. *Int. J. Environ. Pollut.* **2012**, *50*, 308–316. [CrossRef]
18. Oettl, D. *Documentation of the Lagrangian Particle Model GRAL (Graz Lagrangian Model) Vs. 19.01*; Government of Styria Department 15 Energy, Housing, Technology, Air Quality Control: Graz, Austria, 2019.
19. Tinarelli, G.; Mortarini, L.; Trini Castelli, S.; Carlino, G.; Moussafir, J.; Olry, C.; Armand, P.; Anfossi, D. Review and Validation of MicroSpray, a Lagrangian Particle Model of Turbulent Dispersion. In *Lagrangian Modeling of the Atmosphere*; Geophysical Monograph Series; Lin, J., Brunner, D., Gerbig, C., Stohl, A., Luhar, A., Webley, P., Eds.; American Geophysical Union: Washington, DC, USA, 2012; pp. 311–328. [CrossRef]
20. Barbero, D.; Tinarelli, G.; Silibello, C.; Nanni, A.; Gariazzo, C.; Stafoggia, M.; Viegi, G. A microscale hybrid modelling system to assess the air quality over a large portion of a large European city. *Atmos. Environ.* **2021**, *264*, 118656. [CrossRef]
21. Denby, B.R.; Gauss, M.; Wind, P.; Mu, Q.; Grøtting Wærsted, E.; Fagerli, H.; Valdebenito, A.; Klein, H. Description of the uEMEP_v5 downscaling approach for the EMEP MSC-W chemistry transport model. *Geosci. Model Dev.* **2020**, *13*, 6303–6323. [CrossRef]
22. Sanchez, B.; Santiago, J.L.; Martilli, A.; Martin, F.; Borge, R.; Quaassdorff, C.; de la Paz, D. Modelling NOx concentrations through CFD-RANS in an urban hot-spot using high resolution traffic emissions and meteorology from a mesoscale model. *Atmos. Environ.* **2017**, *163*, 155–165. [CrossRef]
23. Tominaga, Y.; Stathopoulos, T. CFD simulation of near-field pollutant dispersion in the urban environment: A review of current modeling techniques. *Atmos. Environ.* **2013**, *79*, 716–730. [CrossRef]
24. Gousseau, P.; Blocken, B.; Stathopoulos, T.; Van Heijst, G.J.F. Near-field pollutant dispersion in an actual urban area: Analysis of the mass transport mechanism by high-resolution Large Eddy Simulations. *Comput. Fluids* **2015**, *114*, 151–162. [CrossRef]
25. Pantusheva, M.; Mitkov, R.; Hristov, P.O.; Petrova-Antonova, D. Air Pollution Dispersion Modelling in Urban Environment Using CFD: A Systematic Review. *Atmosphere* **2022**, *13*, 1640. [CrossRef]
26. Wang, A.; Fallah-Shorshani, M.; Xu, J.; Hatzopoulou, M. Characterizing near-road air pollution using local-scale emission and dispersion models and validation against in-situ measurements. *Atmos. Environ.* **2016**, *142*, 452–464. [CrossRef]
27. Martín, F.; Janssen, S.; Rodrigues, V.; Sousa, J.; Santiago, J.L.; Rivas, E.; Stocker, J.; Jackson, R.; Russo, F.; Villani, M.G.; et al. Using dispersion models at micro-scale to assess long-term air pollution in urban hot spots: A FAIRMODE joint intercomparison exercise for a case study in Antwerp. *Sci. Total Environ.* **2024**, *925*, 171761. [CrossRef] [PubMed]
28. Tewari, M.; Kusaka, H.; Chen, F.; Coirier, W.J.; Kim, S.; Wyszogrodzki, A.A.; Warner, T.T. Impact of coupling a microscale computational fluid dynamics model with a mesoscale model on urban scale contaminant transport and dispersion. *Atmos. Res.* **2010**, *96*, 656–664. [CrossRef]
29. Kadaverugu, R.; Purohit, V.; Matli, C.; Biniwale, R. Improving accuracy in simulation of urban wind flows by dynamic downscaling WRF with OpenFOAM. *Urban Clim.* **2021**, *38*, 100912. [CrossRef]
30. Wang, J.; Wang, L.; You, R. Evaluating a combined WRF and CityFFD method for calculating urban wind distributions. *Build. Environ.* **2023**, *234*, 110205. [CrossRef]
31. Oettl, D. A multiscale modelling methodology applicable for regulatory purposes taking into account effects of complex terrain and buildings on pollutant dispersion: A case study for an inner Alpine basin. *Environ. Sci. Pollut. Res.* **2015**, *22*, 17860–17875. [CrossRef] [PubMed]
32. Almbauer, R.A.; Oettl, D.; Bacher, M.; Sturm, P.J. Simulation of the air quality during a field study for the city of Graz. *Atmos. Environ.* **2000**, *34*, 4581–4594. [CrossRef]
33. Berchet, A.; Zink, K.; Muller, C.; Oettl, D.; Brunner, J.; Emmenegger, L.; Brunner, D. A cost-effective method for simulating city-wide air flow and pollutant dispersion at building resolving scale. *Atmos. Environ.* **2017**, *158*, 181–196. [CrossRef]
34. AAQD, 2008: Directive 2008/50/EC on Ambient Air Quality and Cleaner Air for Europe. Available online: https://eur-lex.europa.eu/legal-content/en/ALL/?uri=CELEX:32008L0050 (accessed on 15 May 2024).
35. Syrakov, D.; Prodanova, M.; Slavov, K.; Etropolska, I.; Ganev, K.; Miloshev, N.; Ljubenov, T. Bulgarian System for Air Pollution Forecast. *J. Intern. Sci. Publ. Ecol. Saf.* **2013**, *7*, 325–334.
36. Syrakov, D.; Etropolska, I.; Prodanova, M.; Slavov, K.; Ganev, K.; Miloshev, N.; Ljubenov, T. Downscaling of Bulgarian chemical weather forecast from Bulgaria region to Sofia city. *AIP Conf. Proc.* **2013**, *1561*, 120–132. [CrossRef]

37. Atanassov, D.; Spassova, S.; Grancharova, D.; Krastev, S.; Yankova, T.; Nikolov, L.; Chakarova, M.; Krasteva, P.; Genov, N.; Stamenov, J.; et al. Air Pollution Monitoring and Modeling System of the Town of Plovdiv (phase I). *J. Environ. Prot. Ecol.* **2006**, *7*, 260–268.
38. Dimitrova, R.; Velizarova, M. Assessment of the Contribution of Different Particulate Matter Sources on Pollution in Sofia City. *Atmosphere* **2021**, *12*, 423. [CrossRef]
39. Sofia Municipality AQ Plan, 2021 Comprehensive Programme for Improvement of Ambient Air Quality of Sofia Municipality for the Period 2021–2026. (In Bulgarian). Available online: https://www.sofia.bg/en/components-environment-air (accessed on 15 May 2024).
40. Petrov, A. Evaluation of OpenFOAM against CODASC wind tunnel database and impact of heating on the flow in an idealised street canyon. *Int. J. Environ. Pollut.* **2019**, *65*, 149–163. [CrossRef]
41. Petrov, A.; Georgieva, E. An Urban Air Pollution Modelling Test: GRAL vs. CUTE-1 case. *AIP Conf. Proc.* **2019**, *2075*, 120007. [CrossRef]
42. Baumann-Stanzer, K.; Andronopoulos, S.; Armand, P.; Berbekar, E.; Efthimiou, G.; Fuka, V.; Gariazzo, C.; Gasparac, G.; Harms, F.; Hellsten, A.; et al. *COST ES1006-Model Evaluation Case Studies: Approach and Results*; COST Office: Brussels, Belgium, 2015; ISBN 987-3-9817334-2-6.
43. White Paper on the Introduction and Effective Operation of Low-Emission Zones for Motor Vehicles on the Territory of the Metropolitan Municipality. 2022. (In Bulgarian). Available online: https://innoair-sofia.eu/images/documents/documents-bg/04_2_1_White_Book_V4_m.pdf (accessed on 15 May 2024).
44. Lee, K.; Bernard, Y.; Dallmann, T.; Broun, C.; Miller, J. Impact of introducing LEZ in Sofia, Report by International Council on Clean Transportation. 2021. (In Bulgarian). Available online: https://theicct.org/publication/impacts-of-a-low-emission-zone-in-sofia/ (accessed on 15 May 2024).
45. WHO, 2021: World Health Organization Global Air Quality Guidelines: Particulate Matter (PM2.5 and PM10), Ozone, Nitrogen Dioxide, Sulfur Dioxide and Carbon Monoxide, World Health Organization. Available online: https://apps.who.int/iris/handle/10665/345329 (accessed on 15 May 2024). License: CC BY-NC-SA 3.0 IGO.
46. Oettl, D. *Documentation of the Prognostic Mesoscale Model GRAMM (Graz Mesoscale Model) Version 20.1*; Amt d. Stmk. Landesregierung, ABT15, Referat Luftreinhaltung: Graz, Austria, 2020; p. 125.
47. Pasquill, F. The estimation of the dispersion of windborne material. *Meteorol. Mag.* **1961**, *90*, 33–49.
48. Gifford, F.A. Turbulent diffusion-typing schemes: A review. *Nucl. Saf.* **1976**, *17*, 68–86.
49. Kurz, C.; Orthofer, R.; Sturm, P.; Kaiser, A.; Uhrner, U.; Reifeltshammer, R.; Rexeis, M. Projection of the air quality in Vienna between 2005 and 2020 for NO2 and PM10. *Urban Clim.* **2014**, *10*, 703–719. [CrossRef]
50. Demetriou, E.; Hadjistassou, C. Lowering mortality risks in urban areas by containing atmospheric pollution. *Environ. Res.* **2022**, *211*, 113096. [CrossRef]
51. Fabbi, S.; Asaro, S.; Bigi, A.; Teggi, S.; Ghermandi, G. Impact of vehicular emissions in an urban area of the Po valley by microscale simulation with the GRAL dispersion model. *IOP Conf. Ser. Earth Environ. Sci.* **2019**, *296*, 012006. [CrossRef]
52. OpenCFD; OpenFOAM. The Open Source Computational Fluid Dynamics (CFD) Toolbox. 2008. Available online: https://www.opencfd.co.uk/openfoam/ (accessed on 15 May 2024).
53. GRAL GUI Manual. Available online: https://gral.tugraz.at/download/documentations/ (accessed on 15 May 2024).
54. INNOAIR Project. Available online: https://innoair-sofia.eu/en/ (accessed on 15 May 2024).
55. Open Data Portal, Ministry of Interior, Topic Transport, Registered Vehicles as of 01.01.2024. Available online: https://data.egov.bg/data/view/619c72a7-fe9d-432a-8fe8-8e034b90fb9c?rpage=1 (accessed on 15 May 2024).
56. EMEP/EEA Air Pollutant Emission Inventory Guidebook, Technical Guidance to Prepare National Emission Inventories, European Environment Agency, Denmark. 2023. Available online: https://www.eea.europa.eu/publications/emep-eea-guidebook-2023 (accessed on 15 May 2024).
57. Murakami, S.; Mochida, A.; Hayashi, Y.; Hibi, K. Numerical simulation of velocity field and diffusion field in an urban area. *Energy Build.* **1991**, *15*, 345–356. [CrossRef]
58. Blocken, B.; Stathopoulos, T.; Carmeliet, J.; Hensen, J.L.M. Application of computational fluid dynamics in building performance simulation for the outdoor environment: An overview. *J. Build. Perform. Simul.* **2011**, *4*, 157–184. [CrossRef]
59. Jeanjean, A.P.R.; Hinchliffe, G.; McMullan, W.A.; Monks, P.S.; Leigh, R.J. A CFD study on the effectiveness of trees to disperse road traffic emissions at a city scale. *Atmos. Environ.* **2015**, *120*, 1–14. [CrossRef]
60. Atanassov, D.; Petrov, A.; Kirova-Galabova, H.; Maneva-Petrova, V.; Neykova, N.; Hristova, E.; Neykova, R.; Tsenova, B. Development of Possible Scenarios on Cultural Shift in Transportation on Air Quality, INNOAIR Report. 2022. Available online: https://innoair-sofia.eu/images/documents/documents-bg/D_6_4_3_Scenarios_pu.pdf (accessed on 15 May 2024).
61. Atanassov, D.; Petrov, A.; Kirova-Galabova, H.; Maneva-Petrova, V.; Neykova, R.; Tsenova, B.; Neykova, N.; Kolarova, M.; Nikolov, V.; Velchev, K. Effect of Cultural Shift in Transport on Air Quality, INNOAIR Report. 2023. Available online: https://innoair-sofia.eu/images/documents/documents-bg/D6_4_4_Effect_p.pdf (accessed on 15 May 2024).
62. Dzhambov, A.M.; Dimitrova, V.; Germanova, N.; Burov, A.; Brezov, D.; Hlebarov, I.; Dimitrova, R. Joint Associations and Path-ways from Greenspace, Traffic-Related Air Pollution, and Noise to Poor Self-Rated General Health: A Population-Based Study in Sofia, Bulgaria. *Environ. Res.* **2023**, *231*, 116087. [CrossRef] [PubMed]

63. Oettl, D. High resolution maps of nitrogen dioxide for the Province of Styria, Austria. *Int. J. Environ. Pollut.* **2014**, *54*, 137–146. [CrossRef]
64. Li, Y.; Li, R.; Guo, D.; Wang, D.; Pan, Y.; Zhang, J.; Yao, R. Numerical Investigation of the Impact of Tall Buildings on Pollutant Dispersion during Stable Stratification. *Atmosphere* **2024**, *15*, 16. [CrossRef]